Inorg. Chem. **2002**, *41*, 989–997

meso Substituent Effects on the Geometric and Electronic Structures of High-Spin and Low-Spin Iron(III) Complexes of Mono-*meso*-Substituted Octaethylporphyrins

Heather Kalish,[†] Jason E. Camp,[†] Marcin Stępień,[‡] Lechosław Latos-Grażyński,*[,‡] Marilyn M. Olmstead,[†] and Alan L. Balch*[,‡,§]

Departments of Chemistry, University of California, Davis, California 95616 and University of Wrocław, Wrocław, Poland

Received October 8, 2001

Introduction of a single *meso* substituent into ClFe^{III}(OEP) or K[(NC)$_2$Fe(OEP)] results in significant changes in the geometric and/or spectroscopic properties of these complexes. The mono-*meso*-substituted iron(III) complexes ClFe^{III}(*meso*-Ph-OEP), ClFe^{III}(*meso*-*n*-Bu-OEP), ClFe^{III}(*meso*-MeO-OEP), ClFe^{III}(*meso*-Cl-OEP), ClFe^{III}(*meso*-NC-OEP), ClFe^{III}(*meso*-HC(O)-OEP), and ClFe^{III}(*meso*-O$_2$N-OEP) have been isolated and characterized by their UV/vis and paramagnetically shifted ^{1}H NMR spectra. The structures of both ClFe^{III}(*meso*-Ph-OEP) and ClFe^{III}(*meso*-NC-OEP) have been determined by X-ray crystallography. Both molecules have five-coordinate structures typical for high-spin ($S = {}^5/_2$) iron(III) complexes. However, the porphyrins themselves no longer have the domed shape seen in ClFe^{III}(OEP), and the N$_4$ coordination environment possesses a slight rectangular distortion. These high-spin, mono-*meso*-substituted iron(III) complexes display ^{1}H NMR spectra in chloroform-*d* solution which indicate that the conformational changes seen in the solid-state structures are altered by normal molecular motion to produce spectra consistent with C_s molecular symmetry. In pyridine solution the high-spin six-coordinate complexes {(py)ClFe^{III}(*meso*-R-OEP)} form. In methanol solution in the presence of excess potassium cyanide, the low-spin six-coordinate complexes K[(NC)$_2$Fe^{III}(*meso*-R-OEP)] form. The ^{1}H NMR spectra of these show that electron-donating substituents produce an upfield relocation of the *meso*-proton chemical shifts. This relocation is interpreted in terms of increased contribution from the less common $(d_{xz},d_{yz})^4(d_{xy})^1$ ground electronic state as the *meso* substituent becomes more electron donating.

Introduction

Naturally occurring hemes have hydrogen atoms at their *meso* positions. Substitution of one of those protons by a different functional group can have a marked effect on the electronic structure and reactivity of the heme. For example, (py)$_2$Fe(OEPO), shown in Chart 1, has an unusual electronic structure that arises from the delocalization of electrons between the metal and ligand.[1−4] In solution, (py)$_2$Fe(OEPO) is also unusually sensitive toward dioxygen, which causes degradation through ring opening of the porphyrin rather than binding to or oxidation of the iron ion.[1,5] Mono-*meso*-methyl hemes undergo oxidation by heme oxygenase, which specifically attacks the methylated *meso* position with remarkable specificity.[6,7] *meso*-Nitroetioheme with its nitro group protruding above and below the heme plane has been used to probe the available space for heme seating in myoglobin and for observing steric factors that may be involved in directing the regiospecificity of heme cleavage.[8] Treatment of low-spin ($S = 0$) (py)$_2$Fe^{II}(*meso*-R-OEP) with hydrogen peroxide results in replacement of the unique R substituent or attack at the *meso*-H sites in a reaction whose specificity depends on the specific R substituent present.[9] The pattern of

[†] University of California.
[‡] University of Wrocław.
[§] E-mail: albalch@ucdavis.edu.

(1) Balch, A. L. *Coord. Chem. Rev.* **2000**, *200−202*, 349.
(2) Morishima, I.; Fujii, H.; Shiro, Y. *J. Am. Chem. Soc.* **1986**, *108*, 3858.
(3) Morishima, I.; Shiro, Y.; Hiroshi, F. *Inorg. Chem.* **1995**, *34*, 1528.
(4) Balch, A. L.; Koerner, R.; Latos-Grażyński, L.; Noll, B. C. *J. Am. Chem. Soc.* **1996**, *118*, 2760.
(5) St Claire, T. N.; Balch, A. L. *Inorg. Chem.* **1999**, *38*, 684.
(6) Torpey, J.; Lee, D. A.; Smith, K. M.; Ortiz de Montellano, P. R. *J. Am. Chem. Soc.* **1996**, *118*, 9172.
(7) Torpey, J.; Ortiz de Montellano, P. R. *J. Biol. Chem.* **1996**, *271*, 26067.
(8) Wang, J.-T.; Li, Y.; Ma, D.; Kalish, H.; Balch, A. L.; La Mar, G. N. *J. Am. Chem. Soc.* **2001**, *123*, 8080.

10.1021/ic011034q CCC: $22.00
Published on Web 01/31/2002

Chart 1

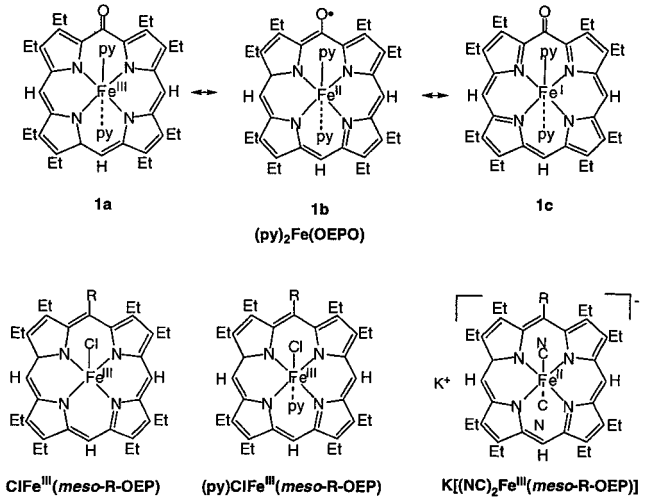

reactivity in this hydrogen peroxide induced reaction indicates that the attacking reagent is nucleophilic.

The environment of the *meso* sites in hemes has been recognized to be sterically constricted.[10] With highly substituted porphyrins such as 2,3,7,8,12,13,17,18-octaethyl-5,10,15,20-tetraphenylporphyrin (H_2OETPP), severe geometric distortions of the porphyrin from planarity can occur. For example, five-coordinate ClFe^{III}(OETPP) shows a pronounced saddle-shaped distortion in its geometric structure.[11,12] Its electronic structure involves some degree of spin admixture of the $S = {}^5/_2$ and ${}^3/_2$ forms, although there is some controversy about the magnitude of the $S = {}^3/_2$ contribution.[11,12]

This article is concerned with the characterization of the geometric and electronic structures of a range of mono-*meso*-substituted octaethylporphyrin complexes of Fe(III). Does the introduction of a single *meso* substituent into octaethylporphyrin alter the geometry of the resulting hemes and produce changes in their electronic structures? The work reported here is part of a project designed to investigate the effects of a non-hydrogen substituent at the *meso* position of a heme on the reactivity of these modified hemes.

Results and Discussion

The mono-*meso*-substituted porphyrins were prepared by known routes and iron inserted to produce ClFe^{III}(*meso*-R-OEP) as outlined in the Experimental Section. The UV/vis spectra of these complexes, which are given in the Experimental Section, are compatible with high-spin, five-coordinate structures for these complexes.

Crystallographic Characterization of ClFe^{III}(*meso*-Ph-OEP) and ClFe^{III}(*meso*-NC-OEP). The structures of both ClFe^{III}(*meso*-Ph-OEP) and ClFe^{III}(*meso*-NC-OEP) have been determined by X-ray crystallography. Figures 1 and 2 show drawings of each of the two molecules. While the structure of ClFe^{III}(*meso*-Ph-OEP) is fully ordered, the structure of ClFe^{III}(*meso*-NC-OEP) is disordered with regard to the position of the cyano group. In the major orientation (with a 0.92 site occupancy) shown in Figure 2, the cyano group is attached to C5, while in the minor orientation (0.08 site occupancy) the cyano group is attached to C20. Selected interatomic distances and angles for both ClFe^{III}(*meso*-Ph-OEP) and ClFe^{III}(*meso*-NC-OEP) are given in Table 1, where they can be compared to those of ClFe^{III}(OEP) (in C_{60}·ClFe^{III}(OEP)·$CHCl_3$),[13] ClFe^{III}(*meso*-O_2N-OEP),[14] and ClFe^{III}(*meso*-CH_3COO-OEP).[15]

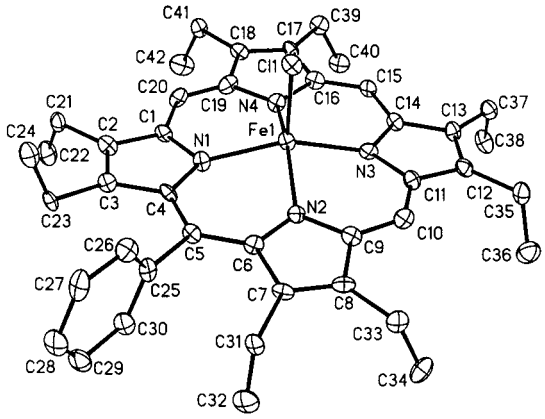

Figure 1. Perspective view of ClFe^{III}(*meso*-Ph-OEP) showing 50% thermal contours.

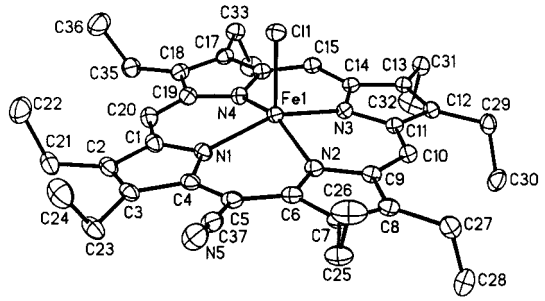

Figure 2. Perspective view of ClFe^{III}(*meso*-CN-OEP) showing 50% thermal contours.

Both molecules shown in Figures 1 and 2 have five-coordinate structures typical for high-spin ($S = {}^5/_2$) iron(III) complexes. The Fe−N bond lengths fall near the range (2.060−2.087 Å) found for this class of heme complexes.[16] Additionally, the distances of the iron atom from the N_4 plane in each complex is in the range (0.39−0.54 Å) seen for other high-spin, five-coordinate iron(III) porphyrin complexes. The Fe−Cl distances are also normal in length.

While aspects of the iron coordination in these unsymmetrically substituted porphyrins are normal, the porphyrins themselves show interesting variations in their structures. The

(9) Kalish, H. R.; Camp, J. E.; Stepień, M.; Latos-Grażyński, L.; Balch, A. L. *J. Am. Chem. Soc.* **2001**, *123*, 11719.
(10) Woodward, R. B. *Angew. Chem.* **1960**, *72*, 651.
(11) Cheng, R.-J.; Chen, P.-Y.; Gau, P.-R.; Chen, C.-C.; Peng, S.-M. *J. Am. Chem. Soc.* **1997**, *119*, 2563.
(12) Schünemann, V.; Gerdan, M.; Trautwein, A. X.; Haoudi, N.; Mandon, D.; Fisher, J.; Weiss, R.; Tabard, A.; Guilard, R. *Angew. Chem., Int. Ed.* **1999**, *38*, 3181.
(13) Olmstead, M. M.; Costa, D. A.; Maitra, K.; Noll, B. C.; Phillips, S. L.; Van Calcar, P. M.; Balch, A. L. *J. Am. Chem. Soc.* **1999**, *121*, 7090.
(14) Senge, M. Personal communication, CCD file, TOYSAB.
(15) Balch, A. L.; Latos-Grażyński, L.; Noll, B. C.; Olmstead, M. M.; Zovinka, E. P. *Inorg. Chem.* **1992**, *31*, 2248.
(16) Scheidt, R. W.; Reed, C. A. *Chem. Rev.* **1981**, *81*, 543.

Table 1. Selected Interatomic Distances and Angles

	$ClFe^{III}$(*meso*-Ph-OEP)	$ClFe^{III}$(*meso*-CN-OEP)	$ClFe^{III}$(OEP)[a]	$ClFe^{III}$(*meso*-O_2N-OEP)[b]	$ClFe^{III}$(*meso*-CH_3COO-OEP)[c]
			Distances (Å)		
Fe−N1	2.044(5)	2.0728(14)	2.073(8)	2.069	2.073(5)
Fe−N2	2.055(5)	2.0705(14)		2.079	2.060(4)
Fe−N3	2.056(5)	2.0661(14)		2.067	2.075(4)
Fe−N4	2.060(4)	2.0638(14)		2.068	2.066(4)
Fe−Cl	2.2175(16)	2.2341(5)	2.235(9)	2.209	2.236(2)
Fe−N4	0.455	0.463	0.492	0.448	0.462
			Angles (deg)		
N1−Fe−N2	85.78(18)	85.71(6)	86.7(4)	86.8	87.9(2)
N2−Fe−N3	88.43(18)	88.37(5)		88.0	86.2(1)
N3−Fe−N4	85.17(18)	86.43(6)		87.2	88.1(2)
N1−Fe−N4	88.95(18)	88.39(6)		87.3	86.2(2)
N1−Fe−N3	153.90(18)	154.42(6)	152.6(6)	156.4	154.9(2)
N2−Fe−N4	153.96(17)	154.74(6)		153.6	153.4(2)
Cl−Fe−N1	103.53(13)	105.05(4)	103.7(3)	103.9	101.1(1)
Cl−Fe−N2	103.16(13)	103.42(4)		106.2	102.4(1)
Cl−Fe−N3	102.57(13)	100.53(4)		99.7	103.9(1)
Cl−Fe−N4	102.86(13)	101.83(4)		110.0	104.2(1)

[a] Data from: Olmstead, M. M.; Costa, D. A.; Maitra, K.; Noll, B. C.; Phillips, S. L.; Van Calcar, P. M.; Balch, A. L. *J. Am. Chem. Soc*. **1999**, *121*, 7090. [b] Data from: Senge, M. Personal communication, CCD file, TOYSAB. [c] Data from: Balch, A. L.; Latos-Grażyński, L.; Noll, B. C.; Olmstead, M. M.; Zovinka, E. P. *Inorg. Chem*. **1992**, *31*, 2248.

presence of a unique *meso* substituent alters the geometry of the ligating N_4 group from nearly square in $ClFe^{III}$(OEP) to slightly rectangular in the *meso*-substituted complexes. This is best appreciated by comparing the nonbonded N···N distances between cis pairs of nitrogen atoms. In $ClFe^{III}$(OEP) there are two unique N···N distances which are nearly equal, 2.848 and 2.847 Å. In $ClFe^{III}$(*meso*-Ph-OEP) the N1···N2 and N3···N4 distances (2.818 and 2.828 Å, respectively) are shorter than the N2···N3 and N1···N4 distances (2.883 and 2.884 Å). In $ClFe^{III}$(*meso*-NC-OEP) and $ClFe^{III}$(*meso*-CH_3COO-OEP) similar compressions and elongations occur. For $ClFe^{III}$(*meso*-NC-OEP) the N1···N2 and N3···N4 distances are 2.790 and 2.785 Å, while the N2···N3 and N1···N4 distances are 2.867 and 2.876 Å. In $ClFe^{III}$(*meso*-CH_3COO-OEP) the distances corresponding to the N1···N2 and N3···N4 separations in the structures reported here are 2.827 and 2.828 Å and the distances corresponding to the N2···N3 and N1···N4 separations are longer: 2.870 and 2.880 Å. For $ClFe^{III}$(*meso*-O_2N-OEP) disorder produces substantial distribution of the nitro group between two sites (two-thirds at a site equivalent to C5 and one-third at a site equivalent to C20) that blurs any effect of this sort.

The presence of the unique *meso* substituent also changes the porphyrin conformation from the domed conformation seen in $ClFe^{III}$(OEP) and in the monoclinic form of $ClFe^{III}$(TPP)[17] to differently distorted forms. Porphyrin distortions from planarity follow the low-frequency normal vibrational modes of the porphyrin and involve *sad*, *ruf*, *dom*, *wav*(*x*), *wav*(*y*), and *pro* deformations.[18,19] Figure 3 shows the out-of-plane displacements (in units of 0.01 Å) of the core atoms for five related iron porphyrins: $ClFe^{III}$(OEP), $ClFe^{III}$(*meso*-Ph-OEP), $ClFe^{III}$(*meso*-NC-OEP), $ClFe^{III}$(*meso*-O_2N-OEP), and $ClFe^{III}$(*meso*-CH_3COO-OEP). Each of the porphyrins in these solids assumes a somewhat different conformation. In comparison to $ClFe^{III}$(OEP), the porphyrin core of $ClFe^{III}$(*meso*-Ph-OEP) is less domed. In $ClFe^{III}$(*meso*-NC-OEP) the porphyrin core assumes a ruf conformation, while $ClFe^{III}$(*meso*-O_2N-OEP) displays a predominant saddle conformation. Finally, $ClFe^{III}$(*meso*-CH_3COO-OEP) shows a weaker saddle distortion. These observations complement the recent work of Scheidt, Shelnut, and co-workers who have shown that one molecule, $(Cl_3CCO_2)Fe^{III}$(OEP), can adopt five diverse conformations in the crystalline state.[20]

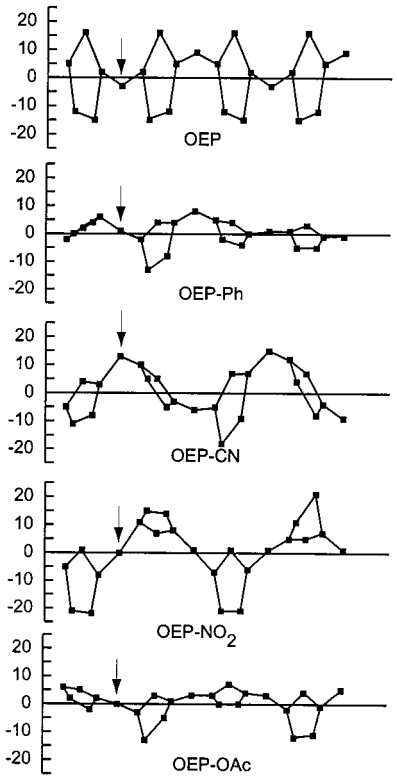

Figure 3. Diagrams showing the out-of-plane displacements of the porphyrin core atoms from the mean plane of the porphyrin. The unique *meso* substituents are attached to the *meso* carbon atoms denoted by arrows.

(17) Scheidt, W. R.; Finnegan, M. G. *Acta Crystallogr*. **1989**, *C45*, 1214.
(18) Jentzen, W.; Song, X.-Z.; Shelnutt, J. A. *J. Phys. Chem. B* **1997**, *101*, 1684.
(19) Shelnutt, J. A.; Song, X.-Z.; Ma, J.-G.; Jia, S.-L.; Jentzen, W.; Medforth, C. J. *Chem. Soc. Rev*. **1998**, *27*, 31.

Chart 2

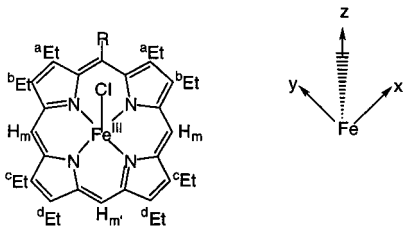

ClFe^{III}(*meso*-R-OEP)

^{1}H NMR Spectra of ClFe^{III}(*meso*-R-OEP). The ^{1}H NMR spectrum of ClFe^{III}(OEP) in chloroform-*d* at 298 K consists of a single *meso* resonance at −55.5 ppm, a doublet for the diastereotopic methylene resonances at 41.6 and 43.7 ppm, and a singlet at 1.5 ppm for the methyl resonances, which is consistent with an earlier study.[21] The temperature dependence of the spectrum almost follows the Curie law (see Supplementary Figure S1). The ^{1}H NMR spectra of complexes of the ClFe^{III}(*meso*-R-OEP) type are similar to that of ClFe^{III}(OEP) but reflect the effects of lower symmetry. As seen in Chart 2,[22] with idealized C_s symmetry ClFe^{III}(*meso*-R-OEP) has four distinct types of ethyl groups and two types of *meso* protons. Since the chloride ligand protrudes from one side of the porphyrin plane, the methylene groups are all diastereotopic. Thus, the symmetry of ClFe^{III}(*meso*-R-OEP) dictates that there should be two *meso* resonances in a 2:1 intensity ratio, eight equally intense methylene resonances, and four equally intense methyl resonances for five-coordinate complexes. Figure 4 shows the spectrum of ClFe^{III}(*meso*-Cl-OEP). (Similar data for ClFe^{III}(*meso*-NC-OEP) are shown in Supplementary Figure S2.) Trace B presents an overview of the spectrum. The two types of *meso* protons produce two broad resonances with a 1:2 intensity ratio in the upfield region, while the methylene protons produce eight resolved resonances of equal intensity in the downfield region. This region is expanded in trace C of Figure 4. Although symmetry dictates that there should be four methyl resonances, there are only three resonances in a 1:2:1 intensity ratio due to accidental overlap of two resonances.

The ^{1}H NMR spectra of the other complexes of this type have related features. Data for ClFe^{III}(*meso*-R-OEP) are collected in Table 2. Figure 5 presents a comparison of the upfield portions of the spectra which contain the resonances of the *meso* protons. While the spectrum of ClFe^{III}(OEP) shows only a single *meso* resonance, the mono-*meso*-substituted complexes—ClFe^{III}(*meso*-Ph-OEP), ClFe^{III}(*meso*-Cl-OEP), ClFe^{III}(*meso*-NC-OEP), and ClFe^{III}(*meso*-O_2N-OEP)—show two resonances in a 2:1 intensity ratio in this region, as expected from their structures. The spectra of ClFe^{III}(*meso*-*n*-Bu-OEP), ClFe^{III}(*meso*-HC(=O)-OEP), and ClFe^{III}(*meso*-MeO-OEP) show additional weak resonances

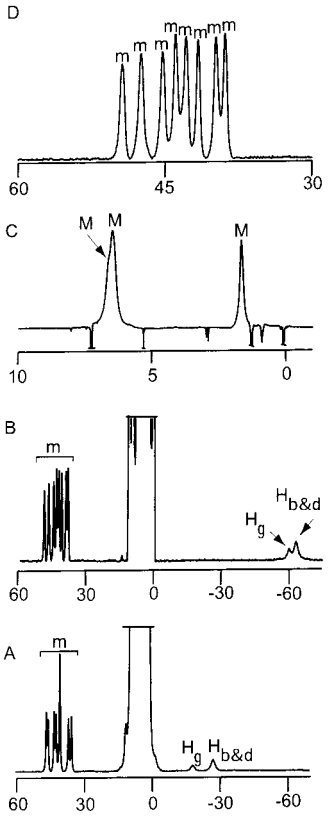

Figure 4. 500 MHz ^{1}H NMR spectra of ClFe^{III}(*meso*-Cl-OEP) at 25 °C. Resonances are labeled $H_{b\&d}$ and H_g for the *meso* protons, M for methyl protons, and m for the methylene protons. Trace A shows the spectrum in pyridine-d_5, B shows the spectrum in chloroform-*d*, C shows the region of the methyl resonances taken under inversion recovery conditions, and D shows an expansion of the methylene region.

in this region. The added resonances result from the presence of a less abundant, rotomeric isomer. With such five-coordinate complexes, the *meso*-*n*-Bu, *meso*-HC(O), and *meso*-MeO substituents can exist in two forms with the substituent protruding on either the same side or the opposite side from the axial chloride ligand. The constricted environment at this *meso* site restricts rotation of these groups about the C−C(*meso*) and O−C(*meso*) bonds. Similar features have been previously observed in the ^{1}H NMR spectrum of ClFe^{III}(*meso*-MeC(=O)O-OEP).[15]

Figure 6 shows the downfield methylene region of the spectra of these complexes. The spectrum of ClFe^{III}(OEP) shows two equally intense resonances in this region. These two resonances are due to the two inequivalent protons of each of the eight symmetrically equivalent methylene groups of the molecule. The spectra of ClFe^{III}(*meso*-NC-OEP) and ClFe^{III}(*meso*-Cl-OEP) show eight equally intense resonances in this region, as expected on the basis of symmetry. The spectra of ClFe^{III}(*meso*-Ph-OEP) and ClFe^{III}(*meso*-O_2N-OEP) are less well resolved, while the spectra of ClFe^{III}(*meso*-*n*-Bu-OEP), ClFe^{III}(*meso*-MeO-OEP), and ClFe^{III}(*meso*-HC(=O)-OEP) show overlapping of the eight resonances of the major isomer and additional smaller peaks due to the presence of a second rotomeric isomer. Note that similar small peaks are also seen in the upfield *meso* region for these complexes.

(20) Neal, T. J.; Cheng, B.; Ma, J.-G.; Shelnut, J. A.; Schultz, C. E.; Scheidt, W. R. *Inorg. Chim. Acta* **1999**, *291*, 49.
(21) Morishima, I.; Kitagawa, S.; Matsuki, E.; Inubushi, T. *J. Am. Chem. Soc.* **1980**, *102*, 2429.
(22) In this chart we use the conventional axis system that is generally employed for metalloporphyrins.

Table 2. Chemical Shifts in ppm for $ClFe^{III}$(*meso*-R-OEP) at 298 K[a,b]

	$ClFe^{III}$(*meso*-R-OEP) in chloroform−d_3				$ClFe^{III}$(*meso*-R-OEP) in pyridine−d_5		
			meso			*meso*	
substituent	methylene	methyl	*cis*	*trans*	methylene	*cis*	*trans*
H	43.7 (8), 41.6 (8)	1.5	−55.5		44.4 (8), 41.6 (8)	−34.2	
butyl	47.3, 42.2	6.7	−57.9	−74.7	46.92, 41.39 (2)	−50.70	−63.51
	38.6, 37.3	6.5	−66.2 i	−78.1 i	38.93, 38.08		
	36.7, 36.3	5.9			37.19, 36.50		
	35.1, 53.2 i				34.83		
	43.9 i, 33.3 i						
	32.6 i						
phenyl	42.4 (2), 41.9	6.5	−65.9	−58.5	42.61, 42.16	−39.53	−29.98
	40.4, 39.3 (2)	6.2			41.81, 40.83		
	38.9, 37.6				40.23 (3), 37.62		
chloro	46.6, 44.5	6.5	−63.7	−60.7	46.43, 45.67	−27.32	−18.24
	42.2, 40.8	6.3			42.97, 42.09		
	39.7, 38.4	1.7			40.42 (2), 36.67		
	36.6, 35.6				35.32		
chloro (axial Br)	45.8, 43.8	6.1	−62.9	−59.9	46.6, 45.8	−26.8	−17.9
	41.6, 40.2	5.9			43.1, 42.2		
	39.1, 37.9				40.5 (2), 36.8		
	36.1, 35.1				35.4		
cyano	46.9, 45.7	6.7	−39.8	−25.3	49.24, 47.92	19.44	10.97
	44.7, 43.5	6.4			45.24, 44.52		
	42.4, 39.7				43.12 (2), 38.36		
	39.4, 38.8				37.32		
nitro	47.6, 44.2	6.7	−57.3	−44.4	49.13, 44.67 (2)	not seen	−3.05
	43.1 (2), 42.3	6.4			43.20, 42.09		
	39.2, 37.9 (2)				40.03, 37.37		
					35.58		
methoxy	43.7, 43.4	6.7	−63	−75	43.88, 42.83	−48.63	−56.97
	42.1 (2), 39.9	6.4			42.02 (2), 40.79	−34.41 i	−46.01 i
	38.0, 37.7	5.9			38.71, 37.24		
	36.3				36.56, 47.52 i		
	49.1 i, 41.2 i				41.61 i, 39.95 i		
	39.3 i						
formyl	44.6, 43.5 (2)	6.5	−51.5	−42.3	46.09, 44.30	−16.20	−6.17
	42.5, 41.3	6.3	−55.6 i	−43.9 i	44.03, 42.30 (2)	−35.56 i	
	40.7, 40.2	5.6			41.94, 40.34		
	39.9, 37.8 i				38.06, 43.61 i		
	34.2 i				40.91 i, 34.83 i		

[1] All resonances are of intensity 1 unless indicated in parentheses. [2] Resonances labeled i correspond to the minor isomer.

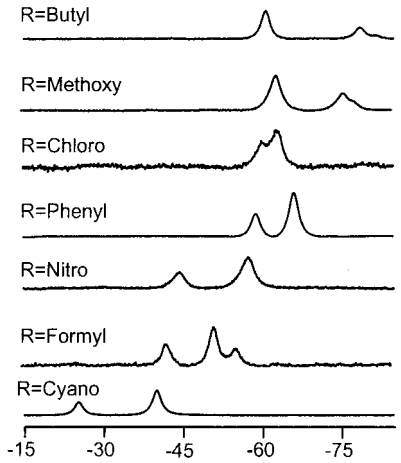

Figure 5. Upfield (*meso*) portion of the 500 MHz ^{1}H NMR spectra of $ClFe^{III}$(*meso*-R-OEP) at 25 °C in chloroform-*d*.

Since a number of studies on the chemical reactivity of these iron porphyrins have been conducted in pyridine solution, the ^{1}H NMR spectra of $ClFe^{III}$(OEP) and $ClFe^{III}$(*meso*-R-OEP) have been examined in pyridine-d_5 solution. As seen in Table 2, the ^{1}H NMR spectrum of $ClFe^{III}$(OEP) in pyridine resembles the spectrum obtained in chloroform with an upfield *meso* resonance and two methylene resonances in the downfield region. The *meso* resonance does show a pronounced downfield shift relative to the corresponding spectrum seen in chloroform-*d*. More importantly, the temperature dependence of the *meso* resonance no longer obeys the Curie law. Figure 7 compares the temperature dependence of the position of the *meso* resonance of $ClFe^{III}$(OEP) in pyridine-d_5 solution with its behavior in chloroform-*d* solution in a plot of the observed chemical shift versus the temperature. The anti-Curie behavior of $ClFe^{III}$(OEP) in pyridine solution is ascribed to the formation of six-coordinate (py)$ClFe^{III}$(OEP) via the equilibrium shown in eq 1. Previous reports have shown that

$$ClFe^{III}(\textit{meso}\text{-R-OEP}) + py \rightleftharpoons (py)ClFe^{III}(\textit{meso}\text{-R-OEP}) \quad (1)$$

the *meso* resonances of Fe^{III} porphyrins are sensitive to the axial ligation, with five-coordinate complexes producing upfield *meso* resonances and six-coordinate complexes producing downfield-shifted *meso* resonances.[23−25] Consequently, the data in Figure 7 are consistent with the influence of the equilibrium shown in eq 1 on the position of the *meso*

(23) Morishima, I.; Shiro, Y.; Wakino, T. *J. Am. Chem. Soc*. **1985**, *107*, 1063.
(24) Zobrist, A.; La Mar, G. N. *J. Am. Chem. Soc*. **1978**, *100*, 1944.
(25) Budd, D. L.; La Mar, G. N.; Langry, K. C.; Smith, K. M.; Nayyir-Mazhir, R. *J. Am. Chem. Soc*. **1979**, *101*, 6091.

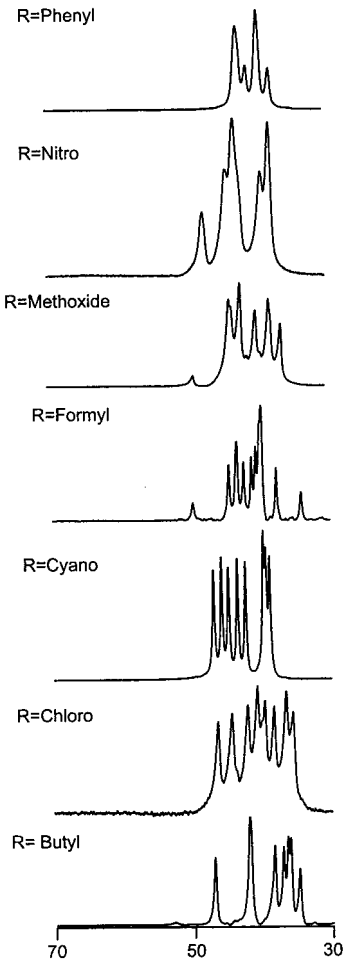

Figure 6. Downfield (methylene) portion of the 500 MHz ^{1}H NMR spectra of ClFe^{III}(*meso*-R-OEP) at 25 °C in chloroform-*d*. Resonance assignments follow those used in Figure 4.

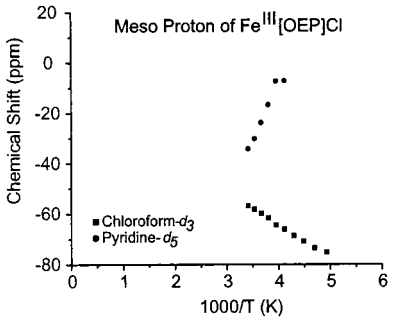

Figure 7. Curie plot (chemical shift versus 1/*T*) of the *meso* resonances for ClFe^{III}(OEP) in chloroform-*d* and pyridine-d_5 solutions.

resonances, with the equilibrium favoring the six-coordinate adduct at low temperature for entropic reasons. This is a dynamic equilibrium which results in observing resonances which represent the average of the five- and six-coordinate forms.

As seen in trace A of Figure 4, the spectrum of ClFe^{III}(*meso*-Cl-OEP) in pyridine-d_5 resembles that obtained in chloroform-*d*, shown in trace B. In both solvents there are eight methylene resonances. Consequently, the two sides of the porphyrin plane are different and the chloride ligand must remain bound. To confirm this conclusion, the spectra of BrFe^{III}(*meso*-Cl-OEP) in chloroform-*d* and pyridine-d_5 have

Table 3. Chemical Shifts in ppm for K[(NC)$_2$Fe^{III}(*meso*-R-OEP)] in Methanol-d_4 at 298 K

meso substituent	substituent peak	methylene	*meso* *trans*	*meso* *cis*
butyl	11.52	between 6.34 and 5.82	−10.46	−17.15
methoxy	12.40	7.47, 7.18 6.50, 6.36	−7.49	−10.74
chloro	none	8.36, 7.92 6.42, 6.11	−3.50	−10.31
phenyl	8.47 ortho 8.11 meta 7.68 para	7.65, 7.21 6.72, 5.95	−0.17	−7.57
nitro	none	9.23, 8.05 5.78, 4.98	4.23	−0.56
cyano	none	9.23, 8.96 6.13, 5.96	5.85	2.23
formyl	11.88	10.05, 8.15 7.90, 6.00	5.50	3.10
hydrogen	3.32[a]	7.35	3.32[a]	3.32[a]

[a] There is only a single *meso*-proton resonance.

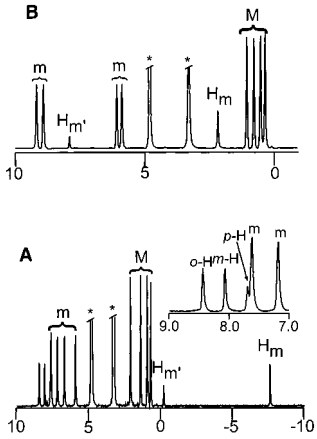

Figure 8. 500 MHz ^{1}H NMR spectra of (A) K[(NC)$_2$Fe^{III}(*meso*-Ph-OEP)] and (B) K[(NC)$_2$Fe^{III}(*meso*-NC-OEP)] in methanol-d_4 at 298 K. The inset shows an expansion of the 9−7 ppm region of the spectrum of K[(NC)$_2$Fe^{III}-(*meso*-Ph-OEP)], where the phenyl resonances occur.

also been examined (see Table 2). In both solvents the spectra of ClFe^{III}(*meso*-Cl-OEP) and BrFe^{III}(*meso*-Cl-OEP) show differences in the chemical shift values for all resonances. This observation is consistent with the axial halide ligands retaining their positions in the coordination sphere of both complexes and in both solvents. In pyridine solution the *meso* resonances for all complexes have undergone a downfield shift in comparison to their positions in chloroform solution (see Table 2). We attribute this downfield shift to the existence of an equilibrium between five-coordinate ClFe^{III}-(*meso*-R-OEP) and six-coordinate (py)ClFe^{III}(*meso*-R-OEP), as shown in eq 1. The temperature dependence of these spectra is also consistent with this hypothesis. Thus, for ClFe^{III}(*meso*-Cl-OEP) the *meso* resonances shift from −27.32 and −18.24 ppm at 298 K to −9.5 and 32 ppm at 243 K.

^{1}H NMR Spectra of K[(NC)$_2$Fe^{III}(*meso*-R-OEP)]. Addition of potassium cyanide in methanol-d_4 to solutions of ClFe^{III}(*meso*-R-OEP) in methanol-d_4 produces solutions of the low-spin complexes K[(NC)$_2$Fe^{III}(*meso*-R-OEP)]. Data from the ^{1}H NMR spectra of these complexes are presented in Table 3. Figure 8 shows representative ^{1}H NMR spectra for solutions of K[(NC)$_2$Fe^{III}(*meso*-NC-OEP)] and K[(NC)$_2$Fe^{III}(*meso*-Ph-OEP)] at 298 K. As expected on the

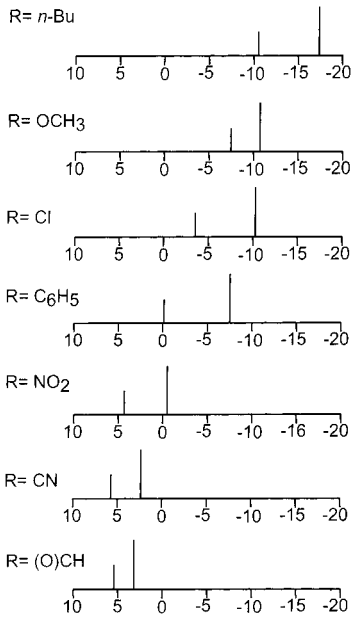

Figure 9. Representative drawings of the 500 MHz ^{1}H NMR spectra of K[$(NC)_2Fe^{III}$(*meso*-R-OEP)], showing the location of the two *meso*-H resonances. For clarity none of the other resonances are shown in these diagrams.

basis of symmetry, the spectrum of each complex consists of four equally intense methylene resonances in the 10−5 ppm region and four equally intense methyl resonances in the 2−0 ppm region. The two types of *meso* protons produce two resonances in a 2:1 intensity ratio, but the observed chemical shifts of these are markedly affected by the unique *meso* substituent, R. For K[$(NC)_2Fe^{III}$(*meso*-Ph-OEP)] the *meso* resonances are found upfield at −0.17 and −7.57 ppm, whereas for K[$(NC)_2Fe^{III}$(*meso*-NC-OEP)] they occur downfield at 7.95 and 2.23 ppm. Additionally the spectrum of K[$(NC)_2Fe^{III}$(*meso*-Ph-OEP)] contains resonances in the 9−7.5 ppm region that are due to the *meso*-phenyl substituent, as seen in inset A. The small hyperfine shifts of these phenyl protons indicate that the dipolar contribution is negligible.

Figure 9 shows the remarkable variation in the chemical shifts of the *meso* resonances in the seven complexes K[$(NC)_2Fe^{III}$(*meso*-R-OEP)], where R is butyl, methoxy, chloro, phenyl, formyl, nitro, and cyano in methanol-d_4 at 298 K. It is clear that the chemical shifts of the *meso* resonances undergo a marked upfield relocation as the π-donating character of the unique *meso* substituent increases.

Discussion

The results presented here indicate that the introduction of a single substituent at one of the *meso* positions of octaethylporphyrin can produce significant changes in the structure and/or spectroscopic features of the resulting iron(III) complexes.

High-Spin Complexes. In terms of structure as seen in Figure 3, the introduction of one *meso* substituent alters the conformation of the porphyrin ligand for high-spin, five-coordinate iron(III) complexes away from the domed conformation seen in $ClFe^{III}$(OEP). However, each *meso* substituent produces a somewhat different structural change. Nevertheless, it is interesting to note that, for the most part, the mono-*meso*-substituted complexes show smaller out-of-plane atom displacements for the porphyrin core atoms than is observed for the unsubstituted parent, $ClFe^{III}$(OEP).

Comparison of the ^{1}H NMR spectra of the high-spin, five-coordinate iron(III) complexes shown in Figure 4 shows that *meso* substitution produces a significant effect on the chemical shifts of the *meso* resonances with electron-withdrawing groups shifting these resonances, and particularly the $H_{m'}$ resonance, in a downfield fashion. These downfield relocations of the *meso* resonances can be quite substantial, as seen in Figure 5. Related work on the effects of β-substitution on the pyrrole rings has shown that substitution has a marked effect upon the chemical shift of the adjacent proton within the same pyrrole ring.[23] In that case, the adjacent pyrrole proton undergoes a downfield shift as the neighboring substituent becomes more electron withdrawing.[26] On the other hand, the chemical shifts of the methylene protons of $ClFe^{III}$(*meso*-R-OEP) show a much smaller effect from the *meso* substituent. These resonances are found in the 35−55 ppm region. The methyl protons are also found to resonate in the narrow window from 0 to 10 ppm.

The typical spin delocalization pathways for high-spin iron(III) porphyrins produce resonances for the β-pyrrole ((TPP)Fe^{III}X) or α-CH_2 ((OEP)Fe^{III}Cl) protons that are strongly shifted downfield. This downfield shift is a result of the σ-contact contribution due to the delocalization through the σ-framework by way of σ-donation to the half-occupied $d_{x^2-y^2}$ iron(III) orbital. Additionally, π-delocalization places a considerable amount of spin density at the *meso* positions. The mechanism is identified as Fe to porphyrin π back-bonding and involves the empty 4e(π^*) orbitals of the porphyrin with a large contribution from the $2p_z$ *meso*-carbon atomic orbitals.[39] The π-spin density delocalized further on produces sign alternation of the contact shift measured for the *meso*-phenyl resonances and is reflected by a large upfield shift of the *meso* protons of (OEP)Fe^{III}Cl. We have noticed previously that the contact shift of high-spin iron(III) *meso*-substituted tetraphenylporphyrins may result from the simultaneous delocalization in σ orbitals as well as in both filled 3e(π) and vacant 4e(π^*) molecular orbitals.[26]

It seems that in (*meso*-R-OEP)Fe^{III}Cl the contribution of the 4e(π^*) related orbitals is systematically varied so that the amount of the π spin density is lowered as the substituent becomes more electron withdrawing. The originally degenerate 4e(π^*) orbitals are split because of the symmetry lowering. The relative amount of spin density located on these orbitals is reversed once we go from the 5-Bu substituent to the 5-CN substituent. The relocations of the *meso*-H resonances seen in Table 2 are simply a reflection of the different pattern of the orbital in question that is produced by the introduction of a unique substituent at one *meso* position.

(26) Wojaczyński, J.; Latos-Grażyński, L.; Hrycyk, W.; Pacholska, E.; Rachlewicz, K.; Szterenberg, L. *Inorg. Chem.* **1996**, *35*, 6861.

The ^{1}H NMR spectra of pyridine solutions of ClFe^{III}(OEP) and ClFe^{III}(*meso*-R-OEP) are indicative of the formation of high-spin, six-coordinate complexes, {(py)ClFe^{III}(OEP)} and {(py)ClFe^{III}(*meso*-R-OEP)}, in which pyridine is added to the coordination site trans to the axial halide. Such mixed-ligand complexes of iron(III) porphyrins are uncommon, but a few well-characterized examples have been isolated and crystallized, including high-spin {(py)(SCN)Fe^{III}(OEPO)}.[27,28] Generally, reactions of pyridine and substituted pyridines with ClFe^{III}P results in the formation of low-spin, six-coordinate $[(py)_2Fe^{III}P]^+$.[29,30] In the work described here, pyridine, a relatively nonpolar solvent, was used, and under these conditions, ionization of the axial halide does not occur. Rather the high-spin, six-coordinate {(py)ClFe^{III}(*meso*-R-OEP)} forms.

Low-Spin Complexes. The spectroscopic results for the low-spin cyano complexes K[(NC)$_2$Fe^{III}(*meso*-R-OEP)] show marked differences which relate to their electronic structures. Low-spin Fe(III) complexes of 4-fold symmetric porphyrins such as H_2TPP and H_2OEP can exist in two different electronic states: the common $(d_{xy})^2(d_{xz},d_{yz})^3$ state and the less common $(d_{xz},d_{yz})^4(d_{xy})^1$ state. However, an increasing number of examples of the less common $(d_{xz},d_{yz})^4(d_{xy})^1$ state have come to light recently.[31−38] For the lower symmetry complexes K[(NC)$_2$Fe^{III}(*meso*-R-OEP)], where one *meso* position is unique, the situation is more complex, and the ground state of K[(NC)$_2$Fe^{III}(*meso*-R-OEP)] combines the features of both ground states with the composition for any one complex controlled by the nature of the *meso*-R substituent. Although we employ the conventional porphyrin-based axis system shown in Chart 2, in the lower symmetry of K[(NC)$_2$Fe^{III}(*meso*-R-OEP)], the d_{xz} and d_{yz} orbitals are no longer strictly degenerate. Nevertheless, we will continue to use the conventional labels $(d_{xy})^2(d_{xz},d_{yz})^3$ and $(d_{xz},d_{yz})^4(d_{xy})^1$ for the two limiting ground-state electronic structures for these low-spin complexes.

The marked upfield shift of the *meso*-proton resonances of of K[(NC)$_2$Fe^{III}(*meso*-R-OEP)] seen in Figure 9 is related to the electronic chaacteristics of the unique *meso* substituent with the presumption that one deals with similar distortion of geometry due to the *meso* substitution. Thus, the most electron donating substituents produce the largest upfield shifts. As a matter of fact, the trend resembles that observed for the high-spin derivative (see above). The gradual nature of the upfield shift probably reflects an incremental change in separation of the energies of the spin-containing orbitals, d_{xy}, d_{xz}, and d_{yz}. The likely dominating factor is the occupancy of the iron d_{xy} orbital as the *meso* substituent becomes more electron donating. The electron-donating substituent can stabilize the d_{xz} and d_{yz} orbitals relative to the d_{xy} orbital by facilitating M-to-L back-donation in the out-of-plane π system. Thus, in the series of complexes studied here, there is a gradual increase in the contribution of the d_{xy} orbital relative to the d_{xz} and d_{yz} orbitals to the electronic structure as the unique *meso* substituent becomes more electron donating. As a result, the *meso* resonances (H_m and $H_{m'}$) relocate in an upfield direction. The upfield *meso*-proton shift seen for iron porphyrins with the $(d_{xz},d_{yz})^4(d_{xy})^1$ ground state arises from the presence of spin in the a_{2u}-like porphyrin orbital, which has principal contributions at the *meso* positions and little or no contribution at the pyrrole β positions.[39]

Complexes with the $(d_{xz},d_{yz})^4(d_{xy})^1$ electronic state that involve $(OEP)^{2-}$ as the ligand are rare, but [(*t*-BuNC)$_2$Fe^{III}-(OEP)]$^+$ is one example which is reported to have a nearly pure $(d_{xz},d_{yz})^4(d_{xy})^1$ electronic ground state.[31] The ^{1}H NMR spectrum of [(*t*-BuNC)$_2$Fe^{III}(OEP)]$^+$ shows that the *meso*-protons are shifted relatively far upfield (δ −37 ppm at 303 K).[31] The crystallographic structure of this complex shows that the porphyrin is significantly ruffled. This ruffling allows mixing of the porphyrin π orbitals with the spin-containing d_{xy} iron orbital and places spin in the porphyrin $3a_{2u}$, π-type orbital, which has large electron density at the *meso* positions. Thus, the structural distortion results in transfer of spin from the half occupied, in-plane d_{xy} orbital to the out-of-plane porphyrin π orbital.

A similar path for spin density transfer can operate in the K[(NC)$_2$Fe^{III}(*meso*-R-OEP)] series. However, in this series the nature of the *meso*-R substituent strongly influences the pattern of the modified porphyrin a_{2u}-like orbital, as reflected by the relative amount of spin density at the *meso* positions. Some preference for added spin density at the H_m positions is observed as the contribution from the $(d_{xz},d_{yz})^4(d_{xy})^1$ state is increased, since the H_m protons, rather than the $H_{m'}$ protons, experience the larger upfield relocation as the *meso* substituent becomes electron donating.

Thus, this work has revealed an important *meso* effect on the structure of low-spin iron(III) porphyrins: the presence of a single electron-donating *meso* substituent favors the $(d_{xz},d_{yz})^4(d_{xy})^1$ state when that substituent is electron donating. Factors consistent with this *meso* effect have also been observed in work on *meso*-tetraalkylporphyrins which readily accommodate the less common $(d_{xz},d_{yz})^4(d_{xy})^1$ electronic state.[40] In particular, comparative studies have shown that

(27) Adams, K. M.; Rasmussen, P. G.; Scheidt, W. R.; Hatano, K. *Inorg. Chem.* **1979**, *18*, 1892.
(28) Scheidt, W. R.; Lee, Y. J.; Geiger, D. K.; Taylor, K.; Hatano, K. *J. Am. Chem. Soc.* **1982**, *104*, 3367.
(29) Walker, F. A.; Lo, M.; Ree, M. T. *J. Am. Chem. Soc.* **1976**, *98*, 5552.
(30) Satterlee, J. D.; LaMar, G. N.; Frye, J. S. *J. Am. Chem. Soc.* **1976**, *98*, 7275.
(31) Safo, M. K.; Walker, F. A.; Raitsimring, A. M.; Walters, W. P.; Dolata, D. P.; Debrunner, P. G.; Scheidt, W. R. *J. Am. Chem. Soc.* **1994**, *116*, 7760.
(32) Guillemot, M.; Simonneaux, G. *J. Chem. Soc., Chem. Commun.* **1995**, 2093.
(33) Walker, F. A.; Nasri, H.; Turowska-Tyrk, I.; Mohanrao, K.; Watson, C. T.; Shokhirev, N. V.; Debrunner, P. G.; Scheidt, W. R. *J. Am. Chem. Soc.* **1996**, *118*, 12109.
(34) Wojaczyński, J.; Latos-Grażyński, L.; Glowiak, T. *Inorg. Chem.* **1997**, *36*, 6299.
(35) Nakamure, M.; Ikeute, T.; Fujii, H.; Yoshimure, T. *J. Am. Chem. Soc.* **1997**, *119*, 6284.
(36) Wolowiec, S.; Latos-Grażyński, L.; Mazzanti, M.; Marcon, J.-C. *Inorg. Chem.* **1997**, *36*, 5761.
(37) Wolowiec, S.; Latos-Grażyński, L.; Toronto, D.; Marcon, J.-C. *Inorg. Chem.* **1998**, *37*, 724.
(38) Simonneaux, G.; Schünemann, V.; Morice, C.; Carel, L.; Toupet, L.; Winkler, H.; Trautwein, A. X.; Walker, F. A. *J. Am. Chem. Soc.* **2000**, *122*, 4366.
(39) Walker, F. A. In *The Porphyrin Handbook*; Kadish, K. M., Smith, K. M., Guilard, R., Eds.; Academic Press: New York, 2000; Vol. 5, p 81.

the $(d_{xz},d_{yz})^4(d_{xy})^1$ electronic state is stabilized by various porphyrin ligands in the following order: octaethyl-*meso*-tetraphenylporphyrin ≤ octamethyl-*meso*-tetraphenylporphyrin ≤ *meso*-tetraphenylporphyrin < *meso*-tetra-*n*-propylporphyin, *meso*-tetracyclopropylporphyrin < *meso*-tetraisopropylporphyrin.[41]

In addition to the marked shifts of the *meso*-proton resonances in these low-spin complexes, the introduction of a unique *meso* substituent also alters the pattern of the pyrrole methylene protons. As seen in Table 3, the spread of the methylene resonances (as given as the difference in chemical shifts of the most upfield and most downfield methylene resonance) decreases as the *meso* substituent becomes more electron-donating. Also, there is an upfield relocation of the methylene resonances as the *meso* substituent becomes more electron donating.

Experimental Section

Materials. Octaethylporphyrin and iron(III) octaethylporphyrin chloride were purchased from Mid Century. The mono-*meso*-substituted porphyrins *meso*-NO_2-H_2OEP,[42] *meso*-NC-H_2OEP,[43] *meso*-Cl-H_2OEP,[44] *meso*-MeO-H_2OEP,[45] *meso*-HC(O)-H_2OEP,[46] *meso*-Ph-H_2OEP,[47] and *meso*-*n*-Bu-H_2OEP[47] were prepared as described previously.

Formation of High-Spin ClFe^{III}(*meso*-R-OEP). Iron was inserted by a standard procedure[48] to yield the five-coordinate chloro complexes ClFe^{III}(*meso*-R-OEP), which were isolated as dark green-brown crystals. UV/vis spectra in chloroform (λ_{max}, nm (ϵ, M^{-1} cm^{-1})): ClFe^{III}(*meso*-Ph-OEP), 386 (7.7×10^4), 510 (8.2×10^3), 540 (3.1×10^3), 642 (3.7×10^3); ClFe^{III}(*meso*-*n*-Bu-OEP), 390 (4.4×10^4), 514 (5.0×10^3), 544 (4.4×10^3), 646 (2.0×10^3); ClFe^{III}(*meso*-MeO-OEP), 386 (7.0×10^4), 508 (7.9×10^3), 538 (6.1×10^3), 640 (3.1×10^3); ClFe^{III}(*meso*-Cl-OEP), 388 (7.7×10^4), 512 (8.5×10^3), 542 (6.8×10^3), 646 (3.7×10^3); ClFe^{III}-(*meso*-HC(=O)-OEP), 384(8.7×10^4), 508 (8.4×10^3), 538 (8.2×10^3), 638 (4.4×10^3); ClFe^{III}(*meso*-NC-OEP), 384 (8.2×10^4), 484 (6.9×10^3), 570 (7.2×10^3), 678 (2.5×10^{33}); ClFe^{III}(*meso*-O_2N-OEP), 378 (8.4×10^4), 508 (9.1×10^{33}), 538 (8.6×10^3), 640 (4.3×10^3).

Formation of Low-Spin K[(NC)$_2$Fe^{III}(*meso*-R-OEP)]. At room temperature a methanol-d_4 solution of ClFe^{III}(*meso*-R-OEP) (2−3 mol) was placed in an NMR tube and sealed with a rubber septum.

Table 4. Crystallographic Data

	ClFe^{III}(*meso*-Ph-OEP)	ClFe^{III}(*meso*-CN-OEP)
formula	$C_{42}H_{48}ClFeN_4$	$C_{37}H_{43}ClFe_3N_5$
fw	700.14	649.06
a, Å	9.975(2)	12.6033(5)
b, Å	13.454(3)	13.6049(5)
c, Å	14.799(3)	19.8435(8)
α, deg	113.590(4)	90
β, deg	95.736(5)	103.8230(10)
γ, deg	105.215(5)	90
V, Å^3	1708.5(6)	3304.0(2)
Z	2	4
cryst syst	triclinic	monoclinic
space group	$P\bar{1}$	$P2_1/c$
T, K	90(2)	90(2)
λ, Å	0.710 73 (Mo Kα)	0.710 73 (Mo Kα)
ρ, g/cm^3	1.361	1.305
μ, mm^{-1}	0.557	0.571
max and min transmissn	0.99−0.90	0.96−0.88
R1 (obsd data)[a]	0.066	0.041
wR2 (all data, F^2 refinement)[b]	0.170	0.108

[a] $R1 = \sum||F_o| - |F_c||/\sum|F_o|$, observed data ($>4\sigma F_o$). [b] $wR2 = [\sum[w(F_o^2 - F_c^2)^2]/\sum[w(F_o^2)^2]]^{1/2}$, all data.

A saturated solution of potassium cyanide in methanol-d_4 was added to the solution of the iron complex. The color of the solution went from a dark brown to bright red or greenish brown upon addition of the cyanide solution. The progress of the reaction was followed by ^{1}H NMR spectroscopy.

X-ray Data Collection for ClFe^{III}(*meso*-Ph-OEP) and ClFe^{III}(*meso*-NC-OEP). Crystals were obtained by slow diffusion of *n*-hexane into a chloroform solution of the appropriate complex. The crystals were coated with a light hydrocarbon oil and mounted in the 90 K dinitrogen stream of a Bruker SMART 1000 diffractometer equipped with a CRYO Industries low-temperature apparatus. Intensity data were collected using graphite-monochromated Mo Kα radiation. Crystal data are given in Table 4.

Solution and Structure Refinement. Scattering factors and correction for anomalous dispersion were taken from a standard source.[49] An absorption correction was applied to each structure.[50] The solutions of the structures were determined by direct methods with SHELXS-97 and subsequent cycles of least-squares refinement on F^2 with SHELXL-97.

Instrumentation. ^{1}H NMR spectra were recorded on a Bruker Avance 500 FT spectrometer (^{1}H frequency is 500.13 MHz). The spectra were recorded over a 100 kHz bandwidth with 64K data points and a 5-ms 90° pulse. For a typical spectrum between 500 and 1000 transients were accumulated with a 50 μs delay time. The residual ^{1}H resonances of the solvents were used as a secondary reference.

Acknowledgment. We thank the NIH (Grant GM-26226, A.L.B.) and the Foundation for Polish Science (L.L.-G) for financial support, the NSF (Grant OSTI 97-24412) for partial funding of the 500 MHz NMR spectrometer, and Sigma Xi for Grants in Aid of Research to H.K.

Supporting Information Available: Supplementary figures S1 and S2 and X-ray crystallographic files in CIF format for ClFe^{III}-(*meso*-Ph-OEP) and ClFe^{III}(*meso*-NC-OEP). This material is available free of charge via the Internet at http://pubs.acs.org.

IC011034Q

(40) Ikeue, T.; Ohgo, Y.; Saitoh, T.; Nakamura, M.; Fujii, H.; Yokoyama, M. *J. Am. Chem. Soc*. **2000**, *122*, 4068.
(41) Ikeue, T.; Ohgo, Y.; Saitoh, T.; Yamaguchi, T.; Nakamura, M. *Inorg. Chem* **2001**, *40*, 3423.
(42) Bonnett, R.; Stephenson, G. F. *J. Org. Chem*. **1965**, *30*, 2791.
(43) Johnson, A. W.; Oldfield, D. *J. Chem. Soc*. *C* **1966**, 794.
(44) Bonnett, R.; Gale, A. D.; Stephenson, G. F. *J. Chem. Soc*. *C* **1966**, 1600.
(45) Barnett, G. H.; Hudson, M. F.; McCombie, S. W.; Smith, K. M. *J. Chem. Soc., Perkin Trans. 1* **1973**, 691.
(46) Inhoffen, H. H.; Furhop, J. H.; Voit, A.; Brockman, H. *Ann. Chem.* **1966**, *695*, 133.
(47) Kalisch, W. W.; Senge, M. O. *Angew. Chem., Int. Ed*. **1998**, *37*, 1107.
(48) Adler, A. D.; Longo, F. R.; Kampas, F. *J. Inorg. Nucl. Chem*. **1970**, *32*, 2443.
(49) *International Tables for Crystallography*; Kluwer Academic: Dordrecht, The Netherlands, 1992.
(50) Sheldrick, G. M. SADABS 2.0, 2000.